Optimisation of the Trigger System of the DESY II Test Beam Facility Pixel Beam Telescopes

Robert Hammann, University of Heidelberg, Germany

supervised by Jan Dreyling-Eschweiler and Lennart Huth, DESY

September 4, 2019

Abstract

The trigger system used for the pixel beam telescopes at the DESY II test beam facility consists of four scintillators each connected to one photomultiplier tube (PMT), whose signals are linked to a logic AND in a trigger logic unit (TLU). Triggering as efficiently as possible maximises the yield in the available beam time. For this purpose, in the scope of this summer student project, the trigger system was optimised for the TLU threshold, the PMT voltage and the geometrical overlap of the scintillators. In a first step, the influence of the TLU threshold and the PMT voltage on the rate of a single PMT was evaluated. Based on these results, an automatic optimisation of the PMT voltage and the TLU threshold was developed. Furthermore, a two-axis linear stage was designed in order to precisely adjust the position of the scintillators.
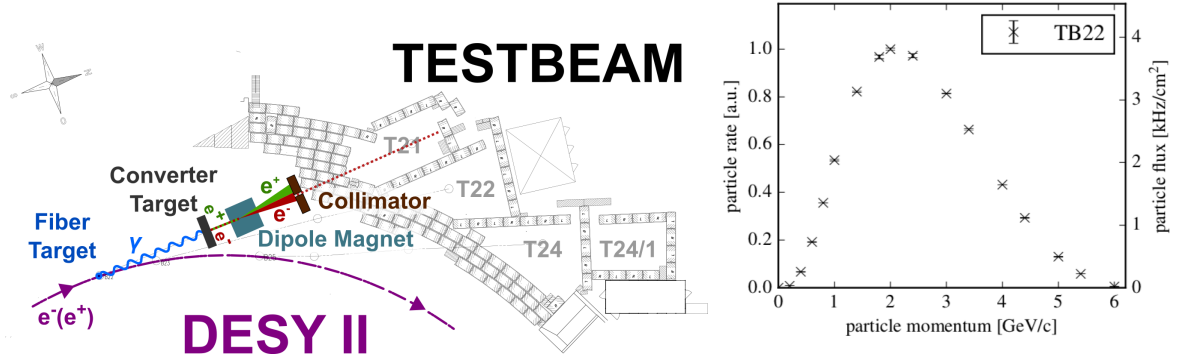
Table of Contents

Figure 1: *Left:* Schematic of the DESY II test beam facility. Single electrons are generated in a two stage process via bremsstrahlung and pair production. The particle momentum/energy can be selected by a dipole magnet. *Right:* Dependency of the electron source rate on the selected particle momentum/energy. The rate is maximal for $p = 2\,\text{GeV/c}$. Both from [1].
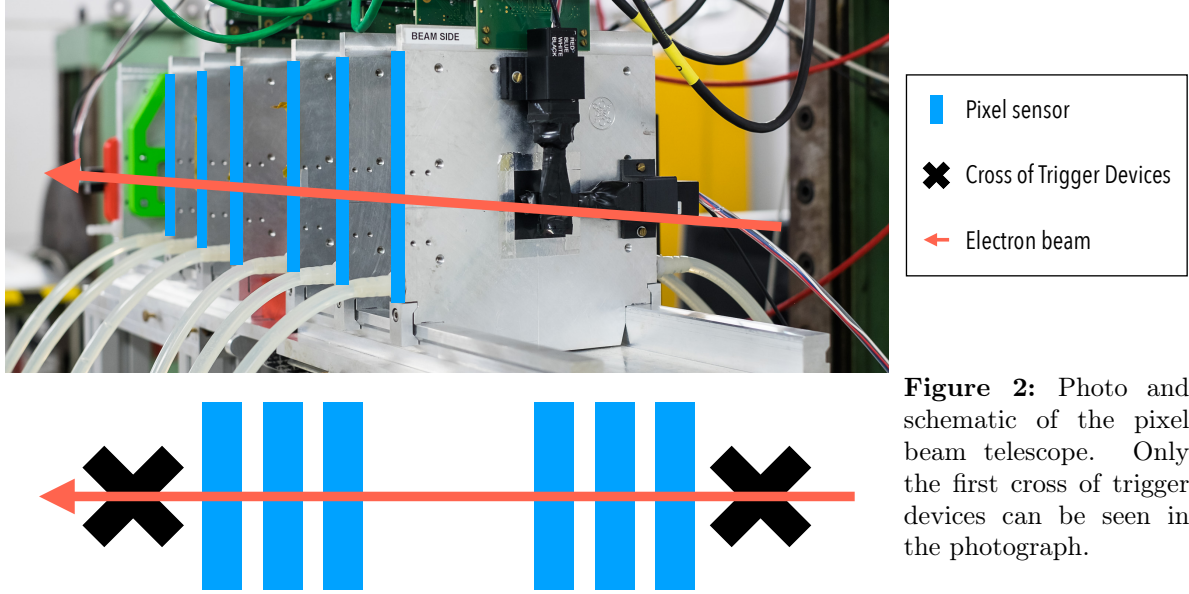
1 Introduction

1.1 The DESY II Test Beam Facility

An essential tool for particle detector research and development are measurements with a test beam in order to asses the functionality and behaviour of a device. The DESY II test beam facility [1] provides a single electron/positron source with a selectable energy[1] from $1\,\text{GeV}$ to $6\,\text{GeV}$ and a particle rate of the order of $\sim 1-10$ kHz. The electron source for this facility is the DESY II synchrotron [2] Single electrons are produced by double conversion as shown in fig. 1 (left). A carbon fiber target is placed in the beam orbit of the synchrotron to produce bremsstrahlung photons that in turn hit a secondary target (e.g. a copper plate of a few mm thickness) creating electron-positron pairs. A primary collimator only lets particles under a certain angle pass, thus allowing for an energy selection with a magnetic dipole. Due to the conversion into bremsstrahlung photons, the rate of particles in the test beam area depends on the selected particle energy, peaking at around $2\,\text{GeV}$ as shown in fig. 1 (right).

1.2 The Pixel Beam Telescope

In order to track the electrons, a EUDET-type pixel beam telescope [3] is provided in each test beam area. It consists of two telescope arms each containing three planes of monolithic active pixel silicon sensors with a very high spatial resolution (here MIMOSA26 [4]) as shown in fig. 2. In the standard configuration, a device under test (DUT) is placed in between the two telescope arms.

---

[1]In the following, energy and momentum will be used synonymously, which is possible since the considered particles are relativistic.

Figure 2: Photo and schematic of the pixel beam telescope. Only the first cross of trigger devices can be seen in the photograph.

1.3 The Trigger System

The pixel sensors only save data, if they receive a trigger signal, which ideally happens whenever an electron passes the pixel beam telescope. In order to register electrons, fast scintillators connected to photomultiplier tubes (PMTs) via light guides are used. In total, four such detectors (two black crosses in fig. 2) are installed. Only if all four detect a coincident signal, a trigger signal is generated and distributed by the trigger logic unit (TLU). The schematics of such a trigger system is shown in fig. 3. Triggering efficiently is important to minimise the amount of collected data while at the same time retain a high statistics of events.

1.3.1 Scintillators

If a particle passes through material it can ionise it. In a scintillator (here a plastic scintillator of the type BC408), the absorbed energy leads to excited molecular states that decay after a short amount of time ($\sim$ ns) by emitting photons of a characteristic wavelength (here UV-range). The number of photons emitted by the scintillator for one particle passing the material depends on the energy loss of this particle due to ionisation, which is described by the Bethe-Bloch formula. For the energy region considered in this project ($1\,\mathrm{GeV}$ - $6\,\mathrm{GeV}$) the dependency of the particle energy on the energy loss is negligible [5]. Additional molecules are added to shift the wavelength of the photons to the visible light range so that they are not absorbed by the scintillator material.
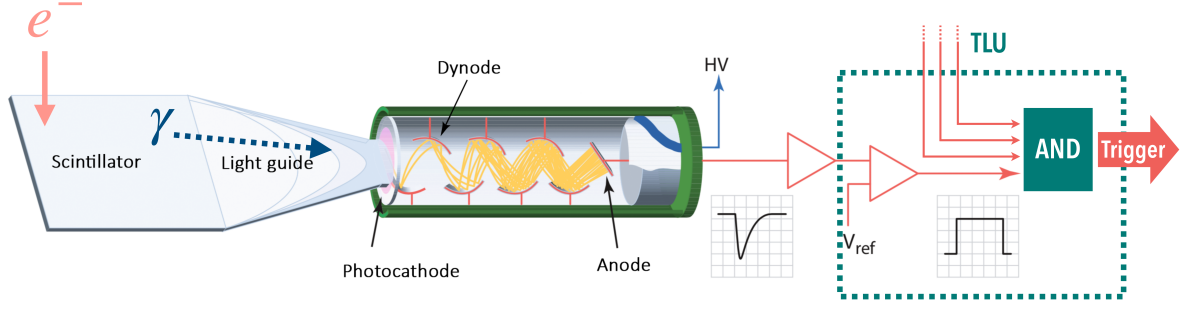
Figure 3: Schematic drawing of the trigger system. One scintillator with an attached PMT as well as the TLU is shown. A passing electron produces UV-photons in the scintillator that in turn produce photoelectrons in the PMTs vacuum tube, which are amplified afterwards. The resulting signal is discriminated against a reference voltage V_{ref} in the TLU. In coincidence mode, the TLU only produces a trigger signal if all four PMT inputs return a signal at the same time. Modified from [6].

1.3.2 Photomultiplier Tubes

In order to convert the photons produced by the scintillator into an electric signal, a Photomultiplier Tube (PMT) [7] is used. It consists of a photocathode and an amplification system of multiple dynodes (anodes) all housed in a vacuum tube. In a first step, an incident photon hits the photocathode and produces a single photoelectron due to the photoelectric effect. This electron is emitted into the vacuum tube and is accelerated to the first dynode by an electric field due to a potential difference. When the electron hits the dynode, multiple secondary electrons are emitted, that in turn are accelerated to the second dynode. This process repeats for all the following dynodes until all secondary electrons are collected at the anode leading to an analogue signal that can be read out. With this avalanche effect, a photoelectron of a single incident photon can be amplified by a factor of $10^5 - 10^7$. The gain can be adjusted by the applied voltage. The high voltage of the PMT used in this project is controlled by an external control voltage between $0.5\,\text{V}$ and $1.1\,\text{V}$. This control voltage will later be referred to as the PMT voltage.

1.3.3 Trigger Logic Unit

If an electron passes the scintillator, a pulse with a certain (negative) amplitude is generated by the PMT as shown in fig. 3. However, for the trigger we are only interested in whether a particle was passing or not. For this, every signal is discriminated against a reference voltage V_{ref} – later referred to as the threshold. To suppress background and to select for electrons that passed all pixel sensors, a trigger signal is only generated and distributed, if all four PMTs detect an event in coincidence. The discrimination and logical linking of the signals as well as the distribution of the trigger signal is done by the trigger logic unit (TLU). This device also allows for setting each PMT voltage and TLU threshold individually. Furthermore, to compensate for different cable lengths, the pulses of each PMT channel can be stretched and delayed individually.

3

1.3.4 Parameters of the Trigger System

There are two parameters of the trigger system that can be adjusted individually for each PMT – the TLU threshold and the PMT voltage. The **TLU threshold** (V_{ref} in fig. 3) corresponds to the sensitivity of the TLU. If this parameter is set too low, no output signal is generated. For a value too close to $0\,\mathrm{V}$, a lot of noise will be accepted. The second parameter is the **PMT voltage**, which corresponds to the gain of the PMT and thus influences the signal amplitude. Since a high PMT voltage results in a short lifetime of the device, in practice, this parameter is kept as low as possible – just high enough to enable distinguishing signal from noise. Currently, default values are used for both of these parameters.

Another parameter which is global for the trigger system is the **geometrical overlap** of the four scintillators. An overlap below 100% inevitably reduces the achievable coincidence rate which corresponds to the trigger rate of the system.

2 Experimental Setup

The measurements for this project were taken at area 22 of the DESY II test beam facility. The experimental setup corresponds to the one shown in fig. 2, however the pixel sensors were not actively used. The measurements shown in the following were taken on five days.

2.1 Data Acquisition

The program written in the scope of this project allows for automatically scanning the TLU thresholds and PMT voltages for all four PMTs in a selectable range and with a selectable number of steps. Also, the acquisition time per data point can be chosen. The measured rates are stored in an ascii file.

2.2 Expected Threshold Dependency

To get an idea of how the choice of the TLU threshold influences the single PMT rate, a histogram of signal amplitudes is simulated as shown in fig. 4 (left). It contains the gaussian distributed signal amplitude from the electrons depositing energy in the scintillator as well as noise with amplitudes close to 0. For any signal amplitude below the threshold[2] , a binary signal is generated by the discriminator. Thus, integrating the signal amplitudes with the threshold as the upper integration limit yields the single PMT rate for this threshold as illustrated in fig. 4 (right). In order to being sensitive to all electron events while rejecting noise, the optimal threshold value is in the center of the plateau.

---

[2]Since the amplitudes are negative, this corresponds to the absolute signal being above the absolute value of the threshold.
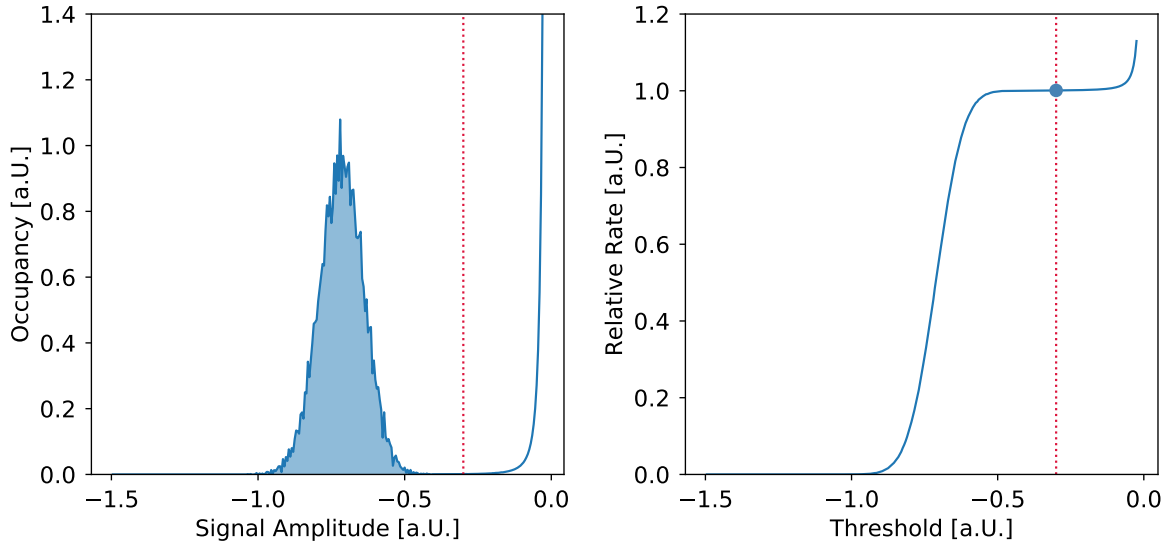
Figure 4: Simulated data. Integrating the gaussian distributed signal amplitude (*left*) up to a threshold value (red dotted line) yields the relative rate for that threshold (*right*). At the center of the plateau, the entire signal is accepted while the background that occurs for lower signal amplitudes is rejected.

3 Experimental Results

In the following, the dependency of the single PMT rate on the TLU threshold and the PMT voltage as well as the influence of the particle energy are studied. Afterwards, the algorithm developed to find optimal parameters for each PMT is discussed. For all measurements, one PMT is kept at a constant voltage and threshold in order to correct the rates of the other PMTs for changes in particle rate provided by the DESY II synchrotron[3]. Thus, all rates shown hereinafter are relative rates. Another effect of this method is, that the acquisition time doubles since a second measurement is required in order to obtain the characteristic for all channels.

3.1 Influence of different Parameters on the single PMT Rate

3.1.1 TLU Threshold

For a constant PMT voltage of $950\,\text{mV}$, the TLU threshold was varied in the range from $-200\,\text{mV}$ to $-10\,\text{mV}$ in 40 equidistant steps. The relative rate is shown in fig. 5 (a, red line). For low threshold values (far away from $0\,\text{mV}$) the relative rate is rather small. For increasing thresholds (closer to $0\,\text{mV}$) the rate increases up to a certain point where one finds a plateau. Increasing the threshold value beyond this point leads to another rise in relative rate. This observation matches the expected behaviour discussed in section 2.2.

---

[3]Since the DESY II synchrotron serves as a pre-accelerator for the PETRA III storage ring, an electron bunch is extracted regularly from DESY II leading to a time with a very low particle rate.
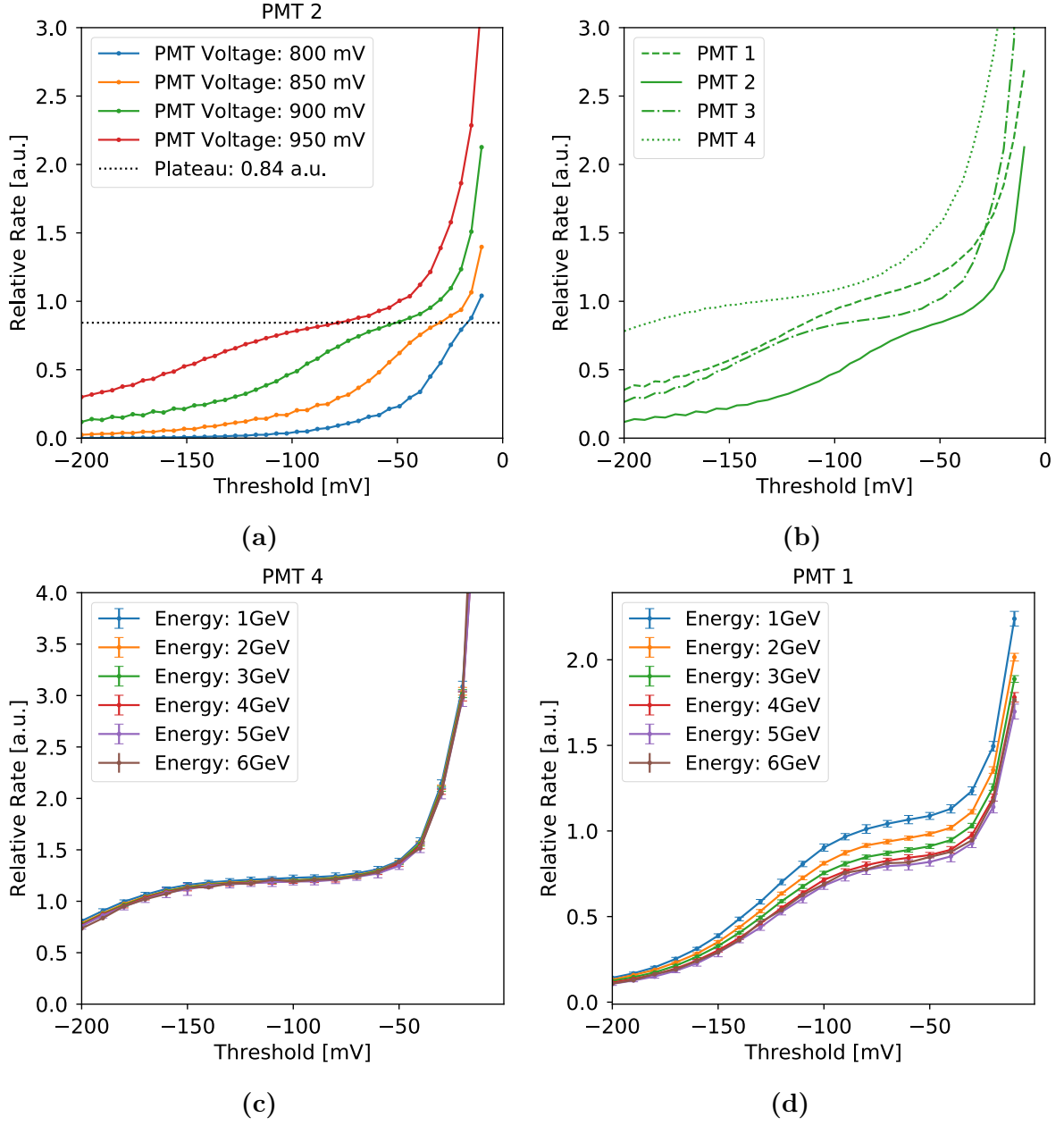
Figure 5: *a)* Dependency of the threshold and the PMT voltage on the relative rate for one PMT. An increase in PMT voltage leads to a broadening of the plateau, which corresponds to an increase of the absolute value of the mean of the signal amplitude. *b)* Measuring the threshold rate curve for different PMTs at a constant voltage of 900 mV yields that different PMTs behave differently. *Bottom:* Dependency of the particle energy on the threshold rate curve for two different PMTs. The errorbars of the measurement at 6 GeV are not drawn to easier see the other errorbars. *c)* For three PMTs the relative rate does not depend on the particle energy. *d)* For one channel a dependency of the energy on the rate was found.

3.1.2 PMT Voltage

In order to evaluate the influence of the PMT voltage on the threshold rate curve discussed in the previous section, the characteristic was acquired for four different voltages ranging from $800\,\mathrm{mV}$ to $950\,\mathrm{mV}$. In fig. 5 (a) for the lowest PMT voltage one can barely see any plateau. For increasing PMT voltages the plateau forms and gets broader while the relative rate at the center of the plateau doesn't change significantly. The broadening of the plateau due to an increasing PMT voltage corresponds to the mean of the gaussian signal shown in fig. 4 (left) to decrease (corresponding to an increase of the absolute signal amplitude) as already discussed in the section 1.3.2. So in principle, as soon as a plateau appears, signal and background can be separated, which can only marginally be improved by increasing the PMT voltage further. A slight positive slope at the center of the plateau can originate from two undistinguishable effects: A background with high amplitude or a signal with a broad signal amplitude distribution. The first corresponds to a low signal to noise ratio (SNR) while the seconds leads to a low PMT efficiency. Comparing different PMTs (fig. 5 b) yields that they behave differently, stressing that using the same default parameters for all connected PMTs can lead to the trigger system operating ineffectively.

3.1.3 Particle Energy

In order to assess the expectation of an energy independent mean of the signal as discussed in section 1.3.1, the threshold rate curve was acquired at constant voltage for six electron energies ranging from $1\,\mathrm{GeV}$ to $6\,\mathrm{GeV}$. For three of the PMTs, the measurement matches the expected behaviour as shown in fig. 5 (c). However, for one PMT the rate decreases for increasing energies as shown in fig. 5 (d). Further measurements are necessary to validate the result and to investigate the origin of this behaviour. Nonetheless, the threshold range of the plateau and thus the optimal threshold value is independent of the energy. Consequently, the optimisation of the parameters can always be conducted at a beam energy of $2\,\mathrm{GeV}$, where the particle rate is maximal according to fig. 1 (right), enabling short optimisation times.

3.2 Optimisation of the Parameters

3.2.1 Threshold and PMT Voltage

Automatically finding the plateau is achieved by fitting a gaussian curve with an offset to the derivative of the measured rate (compare fig. 4, left). Two criteria have to be fulfilled for one data point to be selected as part of the plateau. The threshold has to be above the mean value of the fitted gaussian curve and the derivative has to be below a certain fraction of the sum of the amplitude and the offset of the fitted function. If no such data point was found, the requirements are weakened gradually by increasing the fraction in small steps until one. With this method, the plateau identification gives good results even for narrow plateaus with a constant slope.
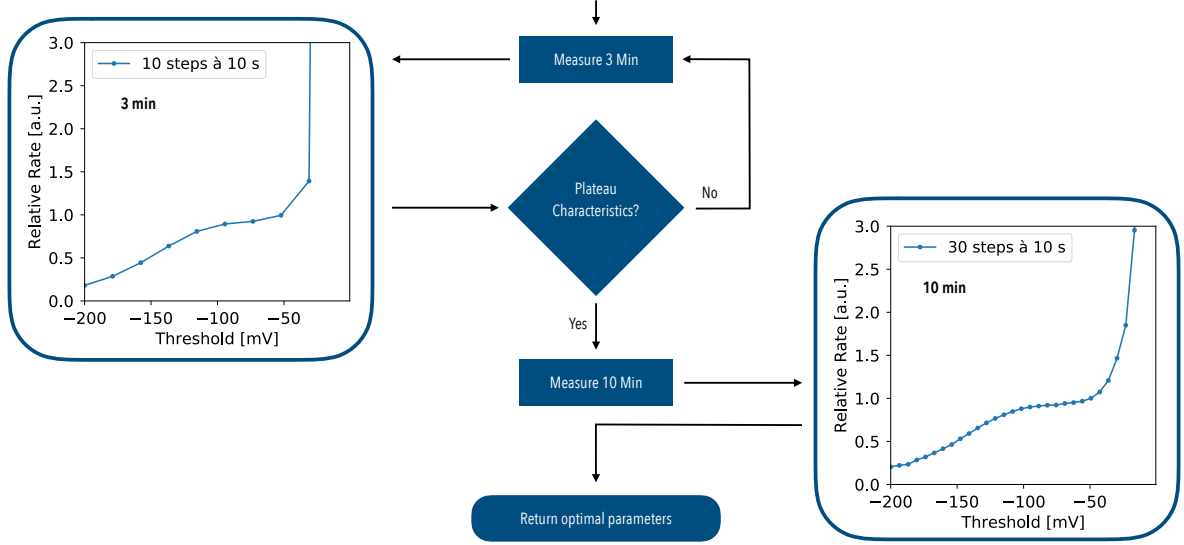
Figure 6: Flow diagram of the implemented optimisation for the TLU threshold and PMT voltage. In a first step, the PMT voltage is increased until a plateau can be seen in three minutes measurements. Afterwards, a more refined threshold rate curve is acquired, allowing the algorithm to determine the optimal threshold value. All four channels are optimised simultaneously.

Additionally, if the previous criteria are not fulfilled for one data point but for its two next neighbours, the data point is also considered to be part of the plateau. This corrects for fluctuations.

Measuring the threshold rate curve for different amounts of threshold steps and acquisition times per step at constant PMT voltage (900 mV) and particle energy (4 GeV), we found that a good approximation of the curve can be achieved with a 10 steps à 10 seconds measurement (approx. 3 minutes due to double measurement). The algorithm for plateau identification still works reliably for a 30 steps à 10 seconds measurement (10 minutes due to double measurement).

Thus, in the implemented optimisation illustrated in fig. 6, first, a three minutes measurement to estimate the shape of the curve. If the plateau can not be seen, this measurement is repeated with different PMT voltages until all of the PMTs show the required characteristic. With the PMT voltages now fixed, a more refined ten minutes measurement is done. With the algorithm developed in this project, the plateau can be identified and the optimal threshold and PMT voltage parameters are returned. For each PMT, the identified plateaus and optimal thresholds for the threshold rate curves at optimal PMT voltages are shown in fig. 7.
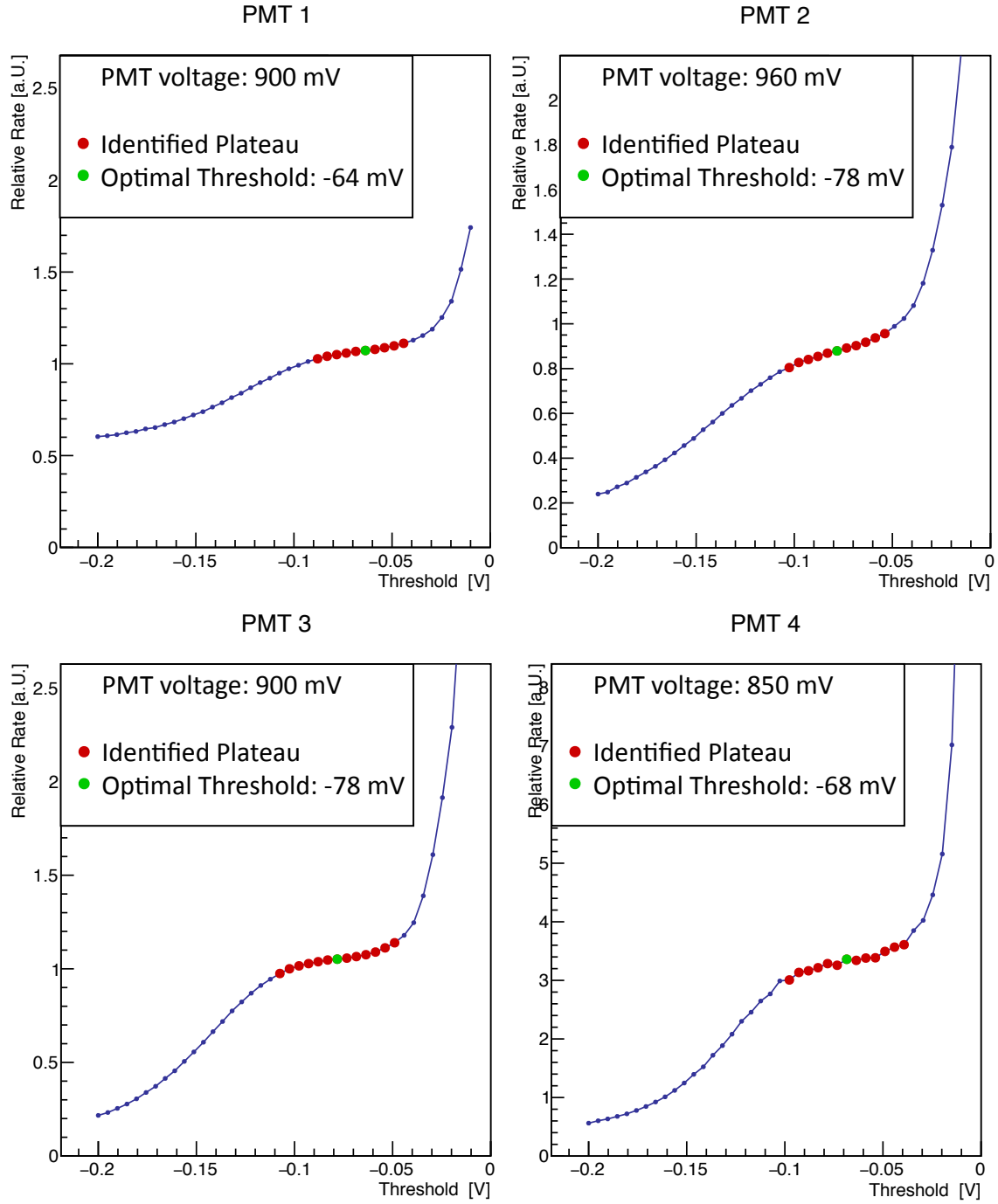
Figure 7: Threshold rate curve at optimal PMT voltages for all PMTs. The plateau identified by the algorithm is indicated in red. The optimal threshold indicated in green is chosen as the center of the identified plateau.
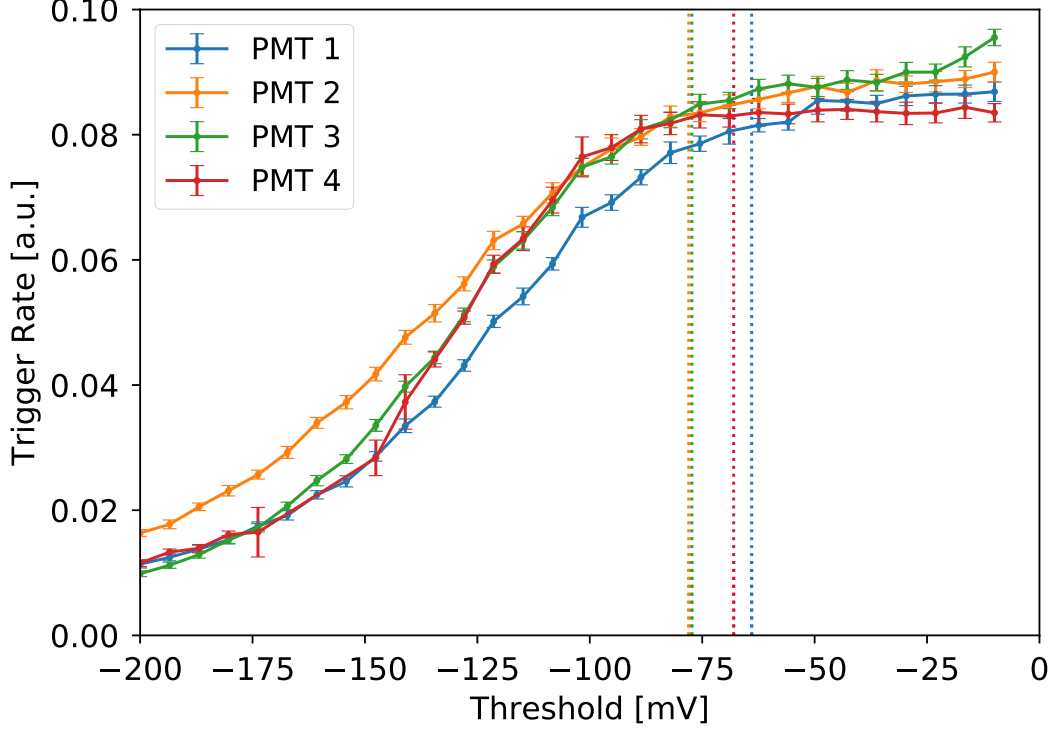
Figure 8: Trigger rate as a function of the TLU threshold varied for one PMT while keeping the other PMTs at optimal values. For thresholds beneath the optimal thresholds (dotted lines), the trigger rate only increases very slightly.

3.2.2 Trigger Rate

In order to test if the parameters found in fig. 7 correspond to a high PMT efficiency, the trigger rate is measured while varying the threshold of one PMT. The other three TLU thresholds as well as all of the PMT voltages are set to the optimum. Repeating these measurements for all four PMTs yields the curves shown in fig. 8. For all PMTs, the trigger rate increases with increasing threshold values up to the optimal threshold (dotted lines). At these points the relative rates for all curves agree with each other within their uncertainties. For PMT 4 a further increase in threshold does not increase the trigger rate. Thus, the parameters found for this PMT are actually the optimal parameters. For the other three PMTs, but especially for PMT 3, a slight increase in trigger rate can be seen. This indicates that the efficiencies of these PMTs at the found optimal parameters are slightly below 100%.

The same measurements have been repeated on a different day, which only partially match the observations discussed here. Further measurements are required to validate the results shown in fig. 8.
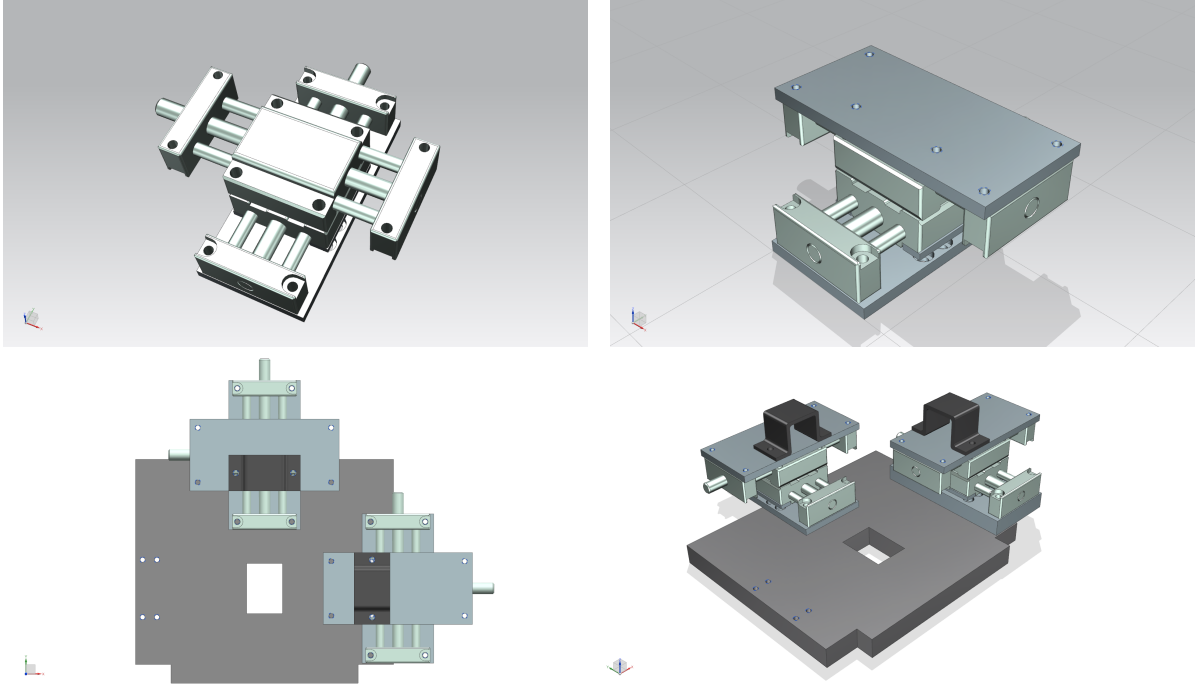
Figure 9: CAD models of the designed two-axis linear stages. *Top:* Single stage without top adaptor plate (left) and with top adaptor plate (right). *Bottom:* Set up of two stages attached to the aluminium frame. Top view (left) and overview (right).

3.3 Geometrical Overlap

The trigger rate is inevitably decreased if the geometrical overlap of the scintillators is not perfect. Thus, to maximise the trigger rate, the positions of the scintillators have to be adjusted precisely. Currently, the position of the scintillators can only be adjusted roughly and along one axis, since the attached PMTs are mounted directly to the aluminium frame of the pixel sensors as shown in fig. 2. In the scope of this project, a two-axis linear stage was developed, which allows to move each scintillator individually in the two dimensions orthogonal to the trajectory of the particle. The CAD model of an individual stage as well as of the final setup is shown in fig. 9. The main components are two linear stages (igus SHTP-01-06-AWM) with a travel range of 37 mm each that are driven by a threaded spindle. These two stages are attached to each other at their sliders at an angle of 90 degrees. Adaptor plates are attached to the top stage and the bottom stage. For the setup, both bottom plates are attached to the aluminium frame in parallel so that the movable stages don't have any contact points.

4 Summary and Outlook

The aim of this summer student project was to optimise the trigger system of the pixel beam telescopes used at the DESY II test beam facility. The influence of the TLU threshold and the PMT voltage on the rate of one single PMT was investigated. For a sufficiently high PMT voltage a plateau of rate was found for a certain threshold range, the middle of which corresponds to the optimal threshold value. Furthermore, the influence of the particle energy on the threshold rate curve was probed. For three of the four PMTs there was no significant difference between the curves in the energy range between $1\,\mathrm{GeV}$ and $6\,\mathrm{GeV}$. For one PMT however, a deviation was discovered. To asses the origin of this unexpected behaviour, further measurements are required.

Based on the results of the previous analysis, an algorithm was developed, which optimises each PMT of the trigger system individually for their PMT voltage and TLU threshold. The results from this part of the project were already used by other experiments conducted at the test beam facility.

Currently, the decision whether a plateau can be seen and how to change the PMT voltage in the first step of the algorithm is made by the user. In principle, this could also be done automatically but to achieve this in a reasonable amount of time, some more profound algorithm is required. Further analysis on the shape of signal and background could improve the choice of the optimal PMT voltages and TLU thresholds. In future studies, one could additionally consider varying stretch and delay of each PMT channel in order to maximise the trigger rate in terms of time.

A chance to halve the optimisation time would be to have a fifth trigger device added to the setup as a reference, which will later not be used for the coincident trigger but can be used to correct the other four devices for fluctuations in particle rate. For this, one could use one of the trigger devices installed to monitor the particle rate in the test beam area.

As a future application one could also test, if the algorithm works reliably for any PMT + scintillator trigger device.

Furthermore, in order to being able to control the geometrical overlap of the scintillators very precisely, a two-axis linear stage was designed, which replaces the fixed PMT holders that are currently being used.

Acknowledgements

First, I would like to thank my project supervisors, Jan Dreyling-Eschweiler and Lennart Huth, for their dedicated and patient supervision and their advise throughout this project. I really enjoyed my work here while still learning a lot.

Further, I would like to thank the test beam group, especially for their help during the test beam week and many interesting discussions.

Finally, thank you to all the fellow summer students – especially my colleague Gonzalo Morras with whom I was working closely together – for making this summer students program so great.

References

[1] R. Diener, J. Dreyling-Eschweiler, et al. The DESY II test beam facility. *Nuclear Instruments and Methods in Physics Research Section A: Accelerators, Spectrometers, Detectors and Associated Equipment*, 922:265 – 286, 2019.

[2] G. Hemmie. DESY II, a new injector for the DESY storage rings PETRA and DORIS II. *IEEE Transactions on Nuclear Science*, 30(4):2028–2030, Aug 1983.

[3] H. Jansen, S. Spannagel, et al. Performance of the EUDET-type beam telescopes. *EPJ Techniques and Instrumentation*, 3(1):7, Oct 2016.

[4] C. Hu-Guo, J. Baudot, et al. First reticule size MAPS with digital output and integrated zero suppression for the EUDET-JRA1 beam telescope. *Nuclear Instruments and Methods in Physics Research Section A: Accelerators, Spectrometers, Detectors and Associated Equipment*, 623(1):480 – 482, 2010. 1st International Conference on Technology and Instrumentation in Particle Physics.

[5] William R. Leo. *Techniques for nuclear and particle physics experiments*. Springer, Berlin ; Heidelberg [u.a.], 1987.

[6] H. Kolanoski and N. Wermes. *Teilchendetektoren*. SpringerLink : Bücher. Springer Spektrum, Berlin, Heidelberg, 1. aufl. 2016 edition, 2016.

[7] Hamamatsu Photonics K.K. *Photomultiplier Tubes*. 2007.